THE JOURNAL OF PHYSICAL CHEMISTRY C

Article

pubs.acs.org/JPCC

Giant Bulk Photovoltaic Effect in Vinylene-Linked Hybrid Heterocyclic Polymer

Published as part of The Journal of Physical Chemistry virtual special issue "Mark S. Gordon Festschrift".

Shi Liu,*[,†] Fan Zheng,[‡] and Andrew M. Rappe*[,‡]

[†]Extreme Materials Initiative, Geophysical Laboratory, Carnegie Institution for Science, Washington, D.C. 20015-1305, United States

[‡]Department of Chemistry, University of Pennsylvania, Philadelphia, Pennsylvania 19104-6323, United States

ABSTRACT: The bulk photovoltaic effect refers to the generation of a steady photocurrent from a homogeneous noncentrosymmetric material. It offers an alternative to the traditional p−n junction-based photovoltaic mechanism to directly convert sunlight to electricity. In this work, we investigate the bulk photovoltaic effect in low-dimensional polar organic materials with first-principles density functional theory calculations and shift current theory. With a strategy designed to break the inversion symmetry along the polymer chain, we demonstrate that conjugated vinylene-linked hybrid heterocyclic polymers can produce a strong bulk photovoltaic response to light, outperforming benchmark inorganic materials. The high current density results from the delocalized wave functions, composed mainly of carbon p orbitals. The great structural and electronic flexibility of polymers offers a robust paradigm to enhance the shift current response through chemical and physical modifications. The development of polymer blends with polymers of different band gaps potentially enables the utilization of the whole visible light spectrum for energy conversion.

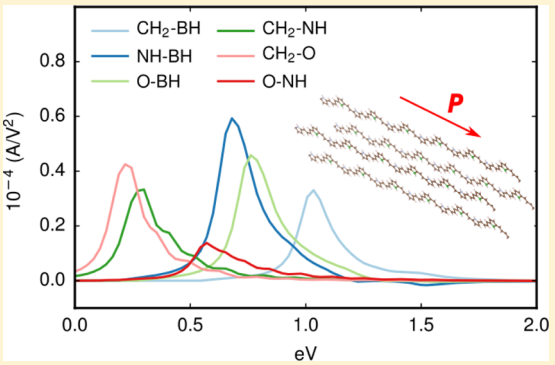

INTRODUCTION

The bulk photovoltaic effect (BPVE) is a phenomenon in which a steady photocurrent and above-band gap photovoltage are generated from a single-phase noncentrosymmetric bulk material.[1−5] This phenomenon was first observed more than 50 years ago in ferroelectric materials[1,2] and modeled theoretically.[6,7] However, the connection between theory and experiment remained poorly understood until recent *ab initio* investigations.[8] The BPVE, in particular, the shift current mechanism,[8] is fundamentally different from the traditional p−n junction-based photovoltaic (PV) mechanism. The driving force that separates photoexcited carriers in a p−n junction solar cell is the built-in electric field at the heterointerface of two semiconductors. In the shift current bulk photovoltaic mechanism, the driving force is the coherent evolution of excited electron (hole) wavepackets. The most attractive feature of the BPVE is the generation of above-band gap photovoltages, which offers a route[9] to overcome the Shockley−Queisser limit of the p−n junction PV technology, where the open-circuit voltage is limited by the fundamental band gap of bulk semiconductors.

Only noncentrosymmetric materials exhibit the BPVE. Ferroelectric materials, characterized by broken inversion symmetry and switchable bulk polarization, guarantee the generation of a bulk photocurrent upon light excitation. However, ferroelectrics often possess large band gaps that prevent the absorption of visible light, causing low conversion efficiency. Recently, there is renewed interest toward applying the BPVE for energy conversion, inspired by the realization of above-band gap open-circuit voltage in ferroelectrics and the synthesis of novel ferroelectrics with band gap in visible light region.[10−15] In particular, $BiFeO_3$ (BFO) is found to exhibit strong photovoltaic response.[16−22] Although various contributions to the photocurrent in BFO were suggested, first-principles calculations demonstrated that the shift current is the main mechanism for the BPVE in single-domain BFO, and the theoretical photoresponse agrees with the measured current magnitudes.[23] In addition to BFO, many low band gap ferroelectrics are also designed and synthesized, with the shift current method applied to evaluate their BPVE performance.[11,24−33] The band gap of BFO (2.7 eV),[34] though smaller than typical ferroelectrics, is still relatively high compared to that of silicon, wasting a large part of the visible light. Therefore, discovering and designing new low band gap materials (polar but not necessarily ferroelectric) with high BPVE is always imperative for the development of solar cells of high power conversion efficiency.

Conjugated organic polymers have been used in many electro-optical devices, such as organic light-emitting diodes,[35,36] photodetectors,[37] and field effect transistors.[38−40] The conjugated organic polymers are also promising candidates for

Received: January 12, 2017
Revised: March 1, 2017
Published: March 2, 2017

DOI: 10.1021/acs.jpcc.7b00374
J. Phys. Chem. C 2017, 121, 6500−6507

next-generation light absorbers in solar cells,[41,42] due to their exceptional properties such as high internal quantum efficiency (photon to electron efficiency),[43] light weight, flexibility, and low synthesis cost. Furthermore, the structural flexibility and tunability of polymers provide a rich playground for the design of functional polymers with desired electronic properties. For example, the band gap of conjugated polymers can be easily tuned by incorporating different donor−acceptor units or by introducing aromatic and quinoid units in an alternating sequence.[44−48] However, there is very limited study of the BPVE in polymeric materials.[12] The BPVE of polyvinylidene fluoride (PVDF), a prototypical organic ferroelectric, was measured more than 30 years ago,[49] but its large band gap and small photocurrent prevent its application to solar energy conversion. Therefore, the design of polymers with small band gaps and strong BPVE is a compelling goal. Though the shift current has been calculated on many nonoxide semiconductors,[50−52] there is little theoretical investigation on low-dimensional materials,[53] although reduced size and dimensionality are predicted to enhance the photoresponse.[9,18] In this work, we compute the shift current responses for various one-dimensional vinylene-linked heterocyclic polymers and find that these polar polymers can generate giant bulk photocurrents along the polymer chain, outperforming benchmark bulk photovoltaic materials such as BFO.

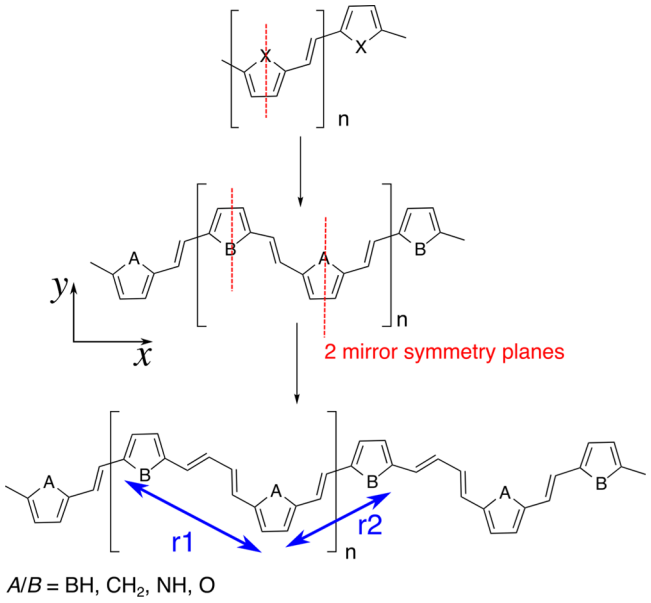

Figure 1. Design of polar hybrid heterocyclic polymers. Starting with a typical heterocyclic polymer with only one type of five-membered ring, the inversion symmetry with respect to the bond center is broken by incorporating two five-membered rings, each bearing a different functional group (A/B = BH, CH_2, NH, and O). Further breaking of rotation and mirror symmetry is accomplished by varying the number of vinylene linkage groups connecting B to A (r1 ≠ r2).

METHODS

Shift current is a second-order nonlinear optical effect with coherent excited states (wave packets) as the carriers, resulting from two successive interactions between the photons and the electrons (or holes).[54] Using perturbation theory, the shift

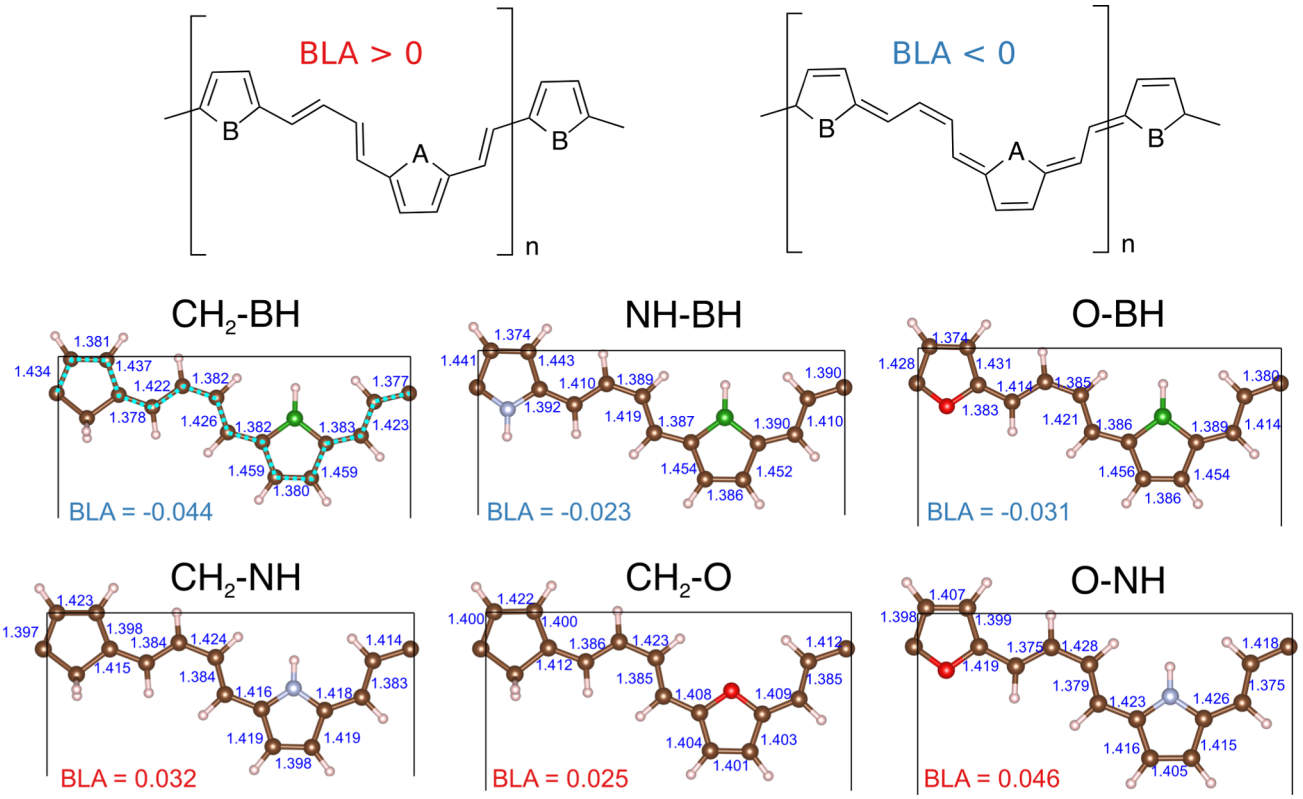

Figure 2. Optimized structures of hybrid heterocyclic polymers with GGA. Bond lengths of C−C bonds (highlighted by broken lines) in Å. The bond length alternation (BLA) is calculated by taking the difference between the bond length of the C−C bond attached to the heterocyclic ring and the C−C bond in the adjacent vinylene linker group. Polymers with boron all have negative values of BLA, showing significant quinoidal character.

DOI: 10.1021/acs.jpcc.7b00374
J. Phys. Chem. C 2017, 121, 6500−6507

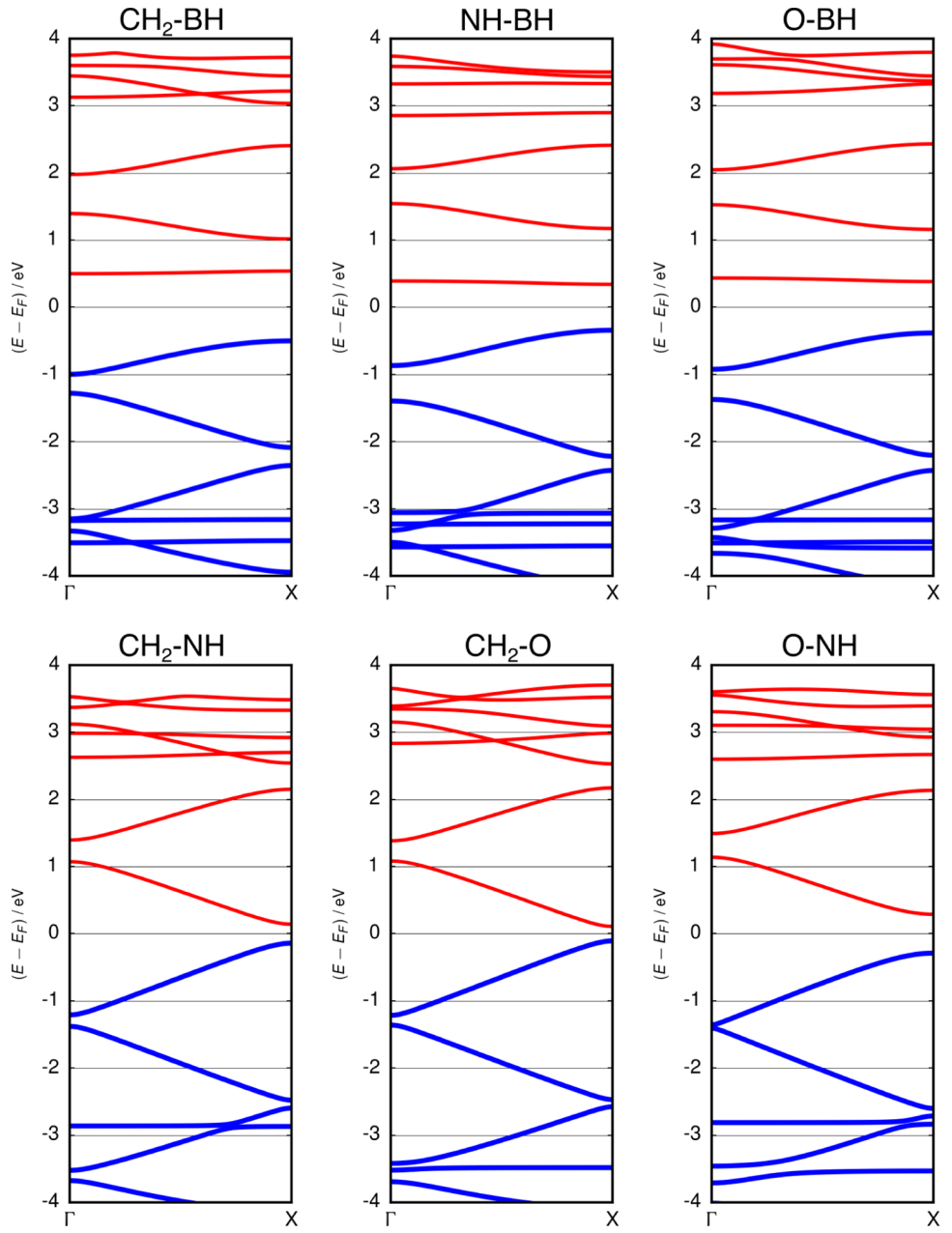

Figure 3. GGA electronic band structures for hybrid heterocyclic polymers (r1 = $(CH)_4$, r2 = $(CH)_2$) along the Γ−X path in the irreducible Brillouin zone. The bandwidth of the lowest conduction band for polymers with the BH functional group is significantly smaller than for polymers without boron.

current response (σ) can be computed from first-principles:

$$J_q = \sigma_{rsq} E_r E_s$$

$$\sigma_{rsq}(\omega) = e \sum_{n',n''} \int \mathrm{d}\mathbf{k}\, \mathcal{I}_{rs}(n',n'',\mathbf{k},\omega)\, \mathcal{R}_q(n',n'',\mathbf{k})$$

$$\mathcal{I}_{rs}(n',n'',\mathbf{k},\omega) = \left(\frac{e}{m\hbar\omega}\right)^2 (f[n''\mathbf{k}] - f[n'\mathbf{k}]) \times \langle n'\mathbf{k}|\hat{P}_r|n''\mathbf{k}\rangle\langle n''\mathbf{k}|\hat{P}_s|n'\mathbf{k}\rangle \times \delta(\omega_{n''}(\mathbf{k}) - \omega_{n'}(\mathbf{k}) \pm \omega)$$

$$\mathcal{R}_q(n',n'',\mathbf{k}) = \left(-\frac{\partial \phi_{n'n''}(\mathbf{k},\mathbf{k})}{\partial k_q} - [\chi_{n''q}(\mathbf{k}) - \chi_{n'q}(\mathbf{k})]\right)$$

where shift current response (σ_{rsq}) is the product of the transition intensity ($\mathcal{I}$) and shift vector ($\mathcal{R}$), representing the probability of excitations and the associated distance for the excited shift current carriers. E_r is the rth component of the electric field of the light, ω is the light frequency, f is the Fermi filling, n and $\mathbf{k}$ are the band index and wavevector of the wave function, respectively, $\phi_{n',n''}$ is the phase of the momentum matrix element for transition from band n' to n'', and χ_n is the Berry connection for the state at band n and $\mathbf{k}$ point.

The plane-wave density functional theory (DFT) code QUANTUM-ESPRESSO is used to optimize the structure and compute the electronic properties of polymers with periodic boundary conditions (PBCs). The generalized gradient approximation (GGA) functional[55] is used with norm-conserving, designed nonlocal pseudopotentials generated with the

DOI: 10.1021/acs.jpcc.7b00374
J. Phys. Chem. C 2017, 121, 6500−6507

OPIUM package.[56,57] In our calculations, a plane-wave cutoff of 50 Ry is sufficient to converge the total energy. To study the single polymer chain, a large box with vacuum more than 10 Å along y and z directions is used to avoid interactions between different images due to PBCs. All the structures are relaxed with a force threshold less than 0.025 eV/Å and an 8 × 2 × 2 k-point grid. With the relaxed structure and the converged charge density, a non-self-consistent calculation on a much denser k-point grid is performed to converge the shift current response. Due to the known deficiency of the GGA functional for band gap predictions, the HSE[58] and B3LYP[59] functionals incorporating exact exchange are used to correct the underestimated band gaps.

RESULTS AND DISCUSSION

Structural Properties. The breaking of inversion symmetry is necessary for the shift current response. However, nonpolar materials (e.g., hexagonal boron nitride) with broken inversion symmetry will only possess shift current under polarized light. Generating shift currents from unpolarized light requires the material to be both noncentrosymmetric and polar. To break the inversion symmetry along the polymer chain, we design vinylene-linked hybrid heterocyclic polymers by incorporating two five-membered rings, each containing a different functional group (A/B). However, this is not sufficient, as the polymer dipole is perpendicular to the chain axis (Figure 1b). We further introduce alternating A−B and B−A distances by increasing the number of vinylene groups connecting B to A (r1, Figure 1c). We explore polymers containing two of the four functional groups, BH, CH_2, NH, and O. It is noted that the BH heterocyclic ring is quinoidal as it has two electrons fewer than the other aromatic heterocyclic rings. The optimized structures are shown in Figure 2. The bond length alternation (BLA), defined as the difference between the length of the nominally single and double bonds along the polymer chain, reflects the π-conjugated behavior. We calculate the BLA for each polymer by taking the difference between the bond length of the C−C bond attached to the heterocyclic ring and the C−C bond in the adjacent vinylene linker group.[48] Within this definition, a positive BLA value suggests aromatic behavior and a negative BLA value indicates quinoidal character (Figure 2). We find that the BH heterocyclic ring gives rise to strong quinoidal character regardless of the type of the other functional group.

Electronic Structure. We investigate the electronic structure of the designed hybrid heterocyclic polymers by calculating the band structures along the Γ−X path in the irreducible Brillouin zone (Figure 3). We find that polymers containing boron (e.g., NH−BH, E_g = 0.68 eV) have larger band gaps at the X point than their counterparts without boron (e.g., NH−O, E_g = 0.58 eV). The larger band gap for polymers with the BH functional group is mainly caused by the reduced bandwidth of the lowest conduction band (CB). For a conjugated polymer, the width of a band reflects the orbital interactions along the polymer chain: a wide dispersive band indicates orbital delocalization and a narrow flat band denotes orbital localization. The small bandwidth of the lowest CB for CH_2−BH, NH−BH, and O−BH polymers is attributed to the highly quinoidal character of the BH cyclic ring, consistent with the BLA analysis.

To provide insights into the electronic structure, we compare the atom-resolved density of states of NH−BH and O−NH polymers (Figure 4). Though orbitals from carbon atoms at the backbone/cyclic rings dominate the states near the Fermi energy, the boron has substantial contributions to band edge states as well, while orbitals from O/N atoms have little contribution. The presence of boron interrupts the p-orbital hybridization of carbon atoms along the polymer chain, thus reducing the electron delocalization and the CB width, increasing the band gap.

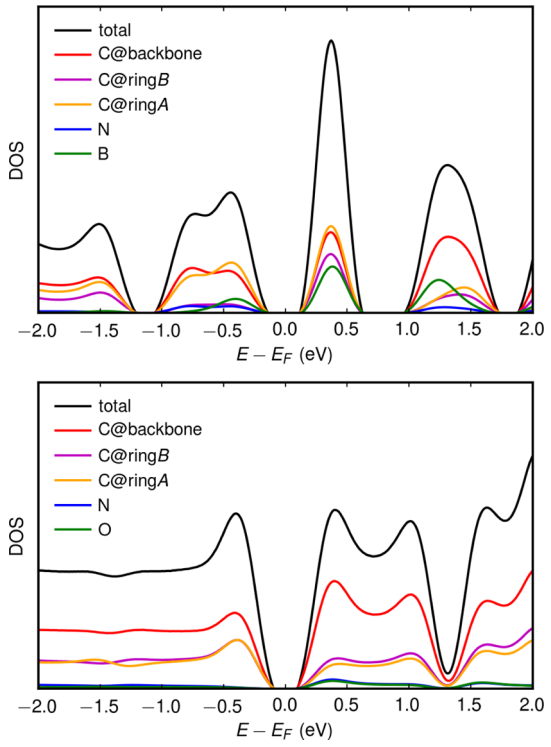

Figure 4. Atom-resolved projected density of states for NH−BH (top) and O−NH (bottom) polymers (r1 = $(CH)_4$, r2 = $(CH)_2$). The boron atom makes substantial contributions to the conduction bands near the Fermi energy.

We further study the bonding character by examining the CB wave functions. As shown in Figure 5, due to the presence of boron, the wave functions and the bonding characters are

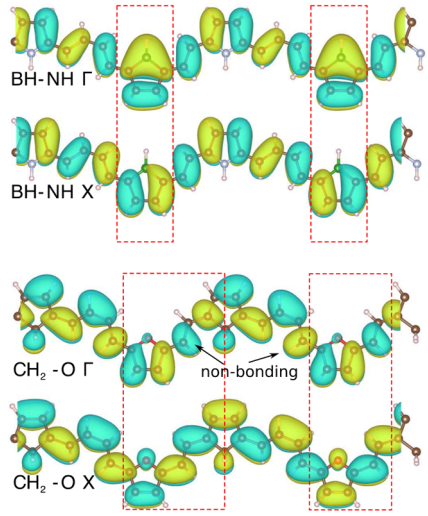

Figure 5. Real-space wave functions at Γ and X points of lowest conduction band for NH−BH and CH_2−O polymers. The rectangular boxes outline the regions where the bonding characters of Γ and X are different. The Γ point wave function of the CH_2−O polymer shows nonbonding carbon atoms, which results in higher orbital energy.

DOI: 10.1021/acs.jpcc.7b00374
J. Phys. Chem. C 2017, 121, 6500−6507

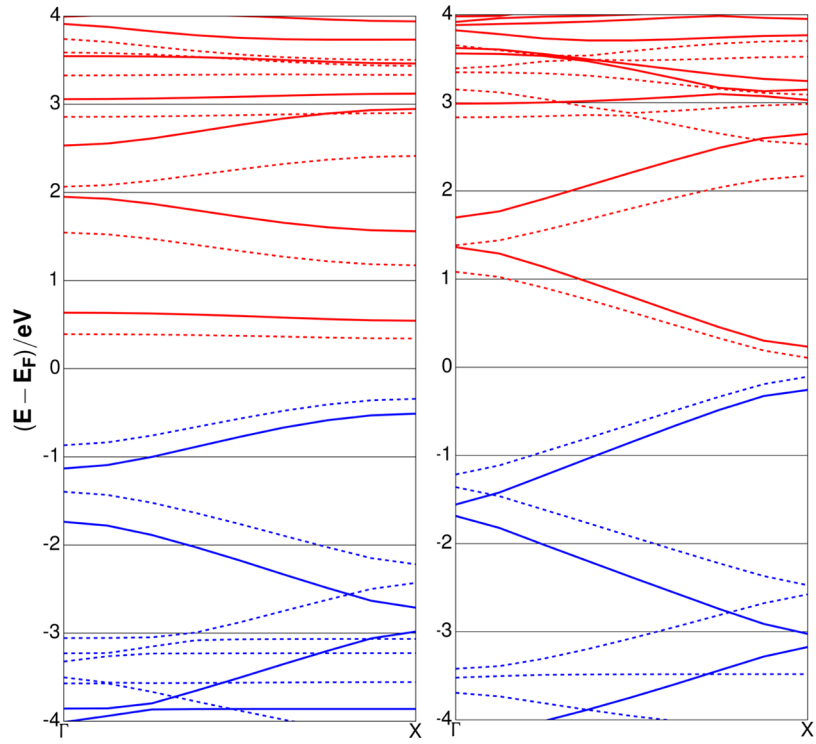

Figure 6. Band structures calculated by HSE (solid line) and GGA (broken line) functionals for (a) NH−BH and (b) CH_2−O. The HSE functional tends to cause a rigid shift of the GGA-calculated bands.

very similar at the Γ and X points, except some small difference within the BH-cyclic ring (outlined by the rectangular boxes), which leads to a modest energy change along the Γ−X path and thus small band dispersion. When BH is replaced with O and NH with CH_2, the bonding character at the Γ point shows a mix of aromatic and quinoidal characters along the chain, but it becomes purely quinoidal at the X point. Moreover, as illustrated from the real-space wave functions, the Γ point wave function shows nonbonding carbon atoms, which further increase its energy. The large difference in bonding characters at the Γ and X points causes a large energy difference and the wide bandwidth.

Because semilocal density functional such as GGA are known to underestimate the band gap, we perform calculations with hybrid density functionals to validate the calculated GGA band structures. Shown in Figure 6 are the band structures obtained with GGA and HSE for NH−BH and CH_2−O polymers. Though the GGA functional underestimates the band gap value almost by half compared to that estimated by HSE, the band dispersions from these two density functionals are similar. Previous studies showed that the B3LYP functional predicts band gap values closer to experimental results for conjugated polymers.[48] We also evaluate the band gaps with the B3LYP functional. We find that the B3LYP further increases the band gap by 0.25 eV compared to HSE results: NH−BH, GGA 0.68 eV, HSE 1.05 eV, B3LYP 1.37 eV; CH_2−O, GGA 0.22 eV, HSE 0.52 eV, B3LYP 0.77 eV. It is noted that the band dispersion from B3LYP is also similar to those obtained with GGA and HSE: in these cases, the exact exchange tends to rigidly shift the GGA bands without changing the orbital characters significantly. For this reason, we decide to compute the shift current response on the basis of the GGA functional due to its low computational cost.

Shift Current Response. We calculate the shift current along the polymer chain in response to both parallel (*xxX*) and perpendicular (*yyX*) linearly polarized light (Figure 7). The studied conjugated polymers all show strong BPVE, with the maximum current response (NH−BH polymer) surpassing the maximum BPVE for inorganic ferroelectric $BiFeO_3$ and solar materials such as $MAPbI_3$. Previous studies suggested that materials characterized by strongly asymmetric and delocalized valence and/or conduction states tend to have larger shift vectors. Typical ferroelectrics such as $PbTiO_3$, although they have large polarization, are not ideal for generating shift currents because the band edge states usually consist of nonbonding, localized states. On the contrary, the delocalized p orbitals along the backbone of conjugated polymers are beneficial for supporting current-carrying excited wavepacket states. The shift current responses of polymers also appear to be highly tunable, as different combinations of functional groups give rise to currents peaking at different light frequencies. A designed polymer blend with different types of hybrid heterocyclic polymers may use the whole visible light spectrum, maximizing the output current from sunlight.

Designed Optimization. The BVPE in vinylene-linked hybrid heterocyclic polymers can be further enhanced with various physical and chemical strategies (Figure 8). Here we demonstrate several possible approaches. First, an increase in the electronegativity difference between A and B functional groups increases the magnitude of symmetry breaking. We find that replacing the hydrogen atom attached to the boron with a $-CF_3$ group results in a larger shift current in the NH−BCF_3 polymer. The second approach is to increase the difference between r1 and r2 by introducing more vinylene linking units between A and B (shown as NH−BH;r1 = $(CH)_8$). We also find that replacing some backbone hydrogen atoms with highly electronegative fluorine atoms (NH−BH;F and NH−BH;r1 = $(CH)_8$ polymers) is beneficial. Lastly, increasing the polymer density per unit volume enhances the response magnitude.

DOI: 10.1021/acs.jpcc.7b00374
J. Phys. Chem. C 2017, 121, 6500−6507

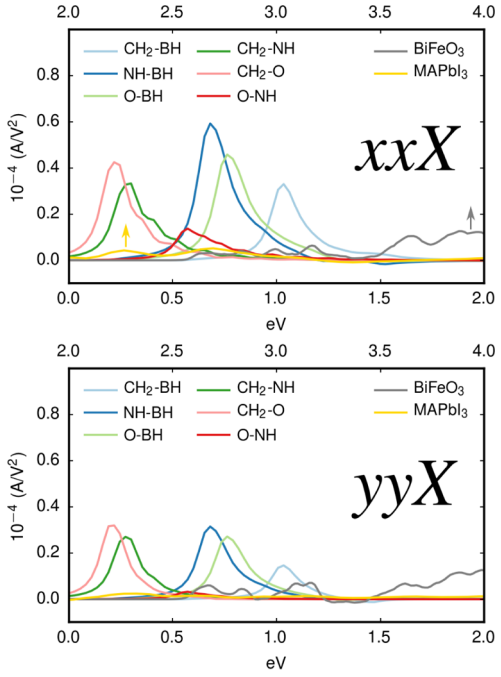

Figure 7. Current density along the polymer chain (X) in response to both parallel (xxX) and perpendicular (yyX) polarized light. The values of current density for benchmark materials, $BiFeO_3$ and $MAPbI_3$, are also presented (top x axis).

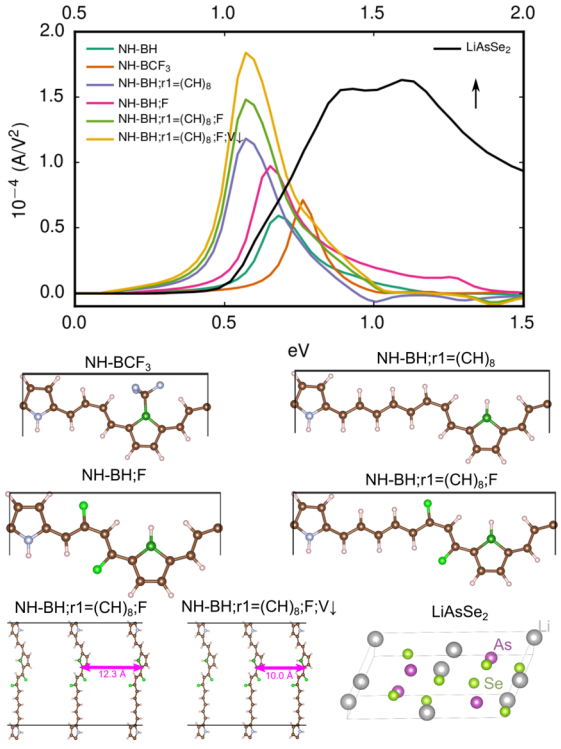

Figure 8. Optimized shift current response through various chemical and physical approaches. Replacing the hydrogen atom attached to the boron with a $-CF_3$ group gives rise to a larger shift current in the NH−BCF_3 polymer. The polymer with a larger difference between r1 and r2 (NH−BH;r1 = $(CH)_8$) also shows a stronger response. Replacing some backbone hydrogen atoms with highly electronegative fluorine atoms (NH−BH;F and NH−BH;r1 = $(CH)_8$;F polymers) is beneficial. Increasing the polymer density per unit volume by reducing interpolymer distance (NH−BH;r1 = $(CH)_8$;F;V↓) enhances the response magnitude.

Through these optimizations, the conjugated polymer can even surpass the peak shift current of the best known inorganic bulk photovoltaic material, $LiAsSe_2$.[50] Because the electron−hole screening is generally weaker in low-dimensional materials,[60,61] additional design principles, such as the usage of substrate of high dielectric constant, can be used to help the suppression of excitonic effect along the polymer chain. It is noted that we assume the polymer chains will pack in parallel direction to maximize the current response in our calculations. Ferroelectric polymers such as PVDF can form polar domains with polymer chains stacked in parallel directions.

CONCLUSION

We computationally designed a series of polar, conjugated polymers by incorporating two different heterocyclic rings and varying the number of vinylene linkage groups. Our first-principles calculations reveal that the presence of boron gives rise to strong quinoidal character, which has a strong influence on the conduction band dispersion and band gap values. All studied polymers possess very high BPVE response, surpassing benchmark materials such as $BiFeO_3$ and $MAPbI_3$, due to the diffuse, delocalized p states at the band edge. The band gaps of the conjugated polymers can easily be tuned by choosing different functional groups in the heterocyclic rings. We propose several chemical and physical approaches to further enhance the shift current response. One of the expected experimental challenges would be aligning the polar polymer chains to minimize the current cancellation. Further studies, both theory and experiments, are required to reveal the synthetic conditions/approaches to exploit the high BPVE of polymers demonstrated in this work.

AUTHOR INFORMATION

Corresponding Authors

*S. Liu. E-mail: sliu@carnegiescience.edu.

*A. M. Rappe. E-mail: rappe@sas.upenn.edu.

ORCID

Shi Liu: 0000-0002-8488-4848

Notes

The authors declare no competing financial interest.

ACKNOWLEDGMENTS

S.L. and F.Z. contributed equally to this work. S.L. is supported by the Carnegie Institution for Science. This work was supported by the Department of Energy under grant DE-FG02-07ER46431. Computational support was provided by the National Energy Reserch Scientific Computing Center (NERSC).

REFERENCES

(1) Chynoweth, A. G. Surface Space-charge Layers in Barium Titanate. *Phys. Rev.* **1956**, *102*, 705−14.

(2) Chen, F. S. Optically Induced Change of Refractive Indices in $LiNbO_3$ and $LiTaO_3$. *J. Appl. Phys.* **1969**, *40*, 3389−96.

(3) Glass, A. M.; von der Linde, D.; Negran, T. J. High-voltage Bulk Photovoltaic Effect and Photorefractive Process in $LiNbO_3$. *Appl. Phys. Lett.* **1974**, *25*, 233−5.

(4) Fridkin, V.; Grekov, A.; Ionov, P.; Rodin, A.; Savchenko, E.; Mikhailina, K. Photoconductivity in Certain Ferroelectrics. *Ferroelectrics* **1974**, *8*, 433−435.

(5) Fridkin, V. M. Bulk Photovoltaic Effect in Noncentrosymmetric Crystals. *Crystallogr. Rep.* **2001**, *46*, 654−8.

DOI: 10.1021/acs.jpcc.7b00374
J. Phys. Chem. C 2017, 121, 6500−6507

(6) Belinicher, V. I.; Kanaev, I. F.; Malinovsky, V. K.; Sturman, B. Theory of Photogalvanic Effect in Ferroelectrics. *Ferroelectrics* **1978**, *22*, 647−8.
(7) Sturman, B.; Carrascosa, M.; Agullo-Lopez, F. Light-induced Charge Transport in $LiNbO_3$ Crystals. *Phys. Rev. B: Condens. Matter Mater. Phys.* **2008**, *78*, 245114.
(8) Young, S. M.; Rappe, A. M. First Principles Calculation of the Shift Current Photovoltaic Effect in Ferroelectrics. *Phys. Rev. Lett.* **2012**, *109*, 116601.
(9) Spanier, J. E.; Fridkin, V. M.; Rappe, A. M.; Akbashev, A. R.; Polemi, A.; Qi, Y.; Gu, Z.; Young, S. M.; Hawley, C. J.; Imbrenda, D.; Xiao, G.; Bennett-Jackson, A. L.; Johnson, C. L. Power Conversion Efficiency Exceeding the Shockley−Queisser Limit in a Ferroelectric Insulator. *Nat. Photonics* **2016**, *10*, 611−616.
(10) Bennett, J. W.; Grinberg, I.; Rappe, A. M. New Highly Polar Semiconductor Ferroelectrics through d^8 Cation-O Vacancy Substitution into $PbTiO_3$: A Theoretical Study. *J. Am. Chem. Soc.* **2008**, *130*, 17409−12.
(11) Grinberg, I.; West, D. V.; Torres, M.; Gou, G.; Stein, D. M.; Wu, L.; Chen, G.; Gallo, E. M.; Akbashev, A. R.; Davies, P. K.; Spanier, J. E.; Rappe, A. M. Perovskites Oxides for Visible-light-adsorbing Ferroelectric and Photovoltaic Materials. *Nature* **2013**, *503*, 509−512.
(12) Vijayaraghavan, R. K.; Meskers, S. C. J.; Rahim, M. A.; Das, S. Bulk Photovoltaic Effect in an Organic Polar Crystal. *Chem. Commun.* **2014**, *50*, 6530−6533.
(13) Somma, C.; Reimann, K.; Flytzanis, C.; Elsaesser, T.; Woerner, M. High-Field Terahertz Bulk Photovoltaic Effect in Lithium Niobate. *Phys. Rev. Lett.* **2014**, *112*, 146602.
(14) Zenkevich, A.; Matveyev, Y.; Maksimova, K.; Gaynutdinov, R.; Tolstikhina, A.; Fridkin, V. Giant Bulk Photovoltaic Effect in Thin Ferroelectric $BaTiO_3$ Films. *Phys. Rev. B: Condens. Matter Mater. Phys.* **2014**, *90*, 161409.
(15) Pérez-Tomás, A.; Lira-Cantú, M.; Catalan, G. Above-Bandgap Photovoltages in Antiferroelectrics. *Adv. Mater.* **2016**, *28*, 9644.
(16) Choi, T.; Lee, S.; Choi, Y.; Kiryukhin, V.; Cheong, S.-W. Switchable Ferroelectric Diode and Photovoltaic Effect in $BiFeO_3$. *Science* **2009**, *324*, 63−6.
(17) Yang, S.; Seidel, J.; Byrnes, S. J.; Schafer, P.; Yang, C.-H.; Rossel, M.; Yu, P.; Chu, Y.-H.; Scott, J. F.; Ager, J. W.; Martin, L.; Ramesh, R. Above-bandgap Voltages from Ferreoelectric Photovoltaic Devices. *Nat. Nanotechnol.* **2010**, *5*, 143−7.
(18) Alexe, M.; Hesse, D. Tip-enhanced photovoltaic effects in bismuth ferrite. *Nat. Commun.* **2011**, *2*, 256.
(19) Bhatnagar, A.; Roy Chaudhuri, A.; Heon Kim, Y.; Hesse, D.; Alexe, M. Role of Domain Walls in the Abnormal Photovoltaic Effect in $BiFeO_3$. *Nat. Commun.* **2013**, *4*, 2835.
(20) Seidel, J.; Fu, D. Y.; Yang, S. Y.; Alarcon-Llado, E.; Wu, J. Q.; Ramesh, R.; Ager, J. W. Efficient Photovoltaic Current Generation at Ferroelectric Domain Walls. *Phys. Rev. Lett.* **2011**, *107*, 126805.
(21) Ji, W.; Yao, K.; Liang, Y. C. Evidence of Bulk Photovoltaic Effect and Large Tensor Coefficient in Ferroelectric $BiFeO_3$ Thin Films. *Phys. Rev. B: Condens. Matter Mater. Phys.* **2011**, *84*, 094115.
(22) Yang, S. Y.; et al. Photovoltaic Effects in $BiFeO_3$. *Appl. Phys. Lett.* **2009**, *95*, 062909.
(23) Young, S. M.; Zheng, F.; Rappe, A. M. First-Principles Calculation of the Bulk Photovoltaic Effect in Bismuth Ferrite. *Phys. Rev. Lett.* **2012**, *109*, 236601.
(24) Nechache, R.; Harnagea, C.; Licoccia, S.; Traversa, E.; Ruediger, A.; Pignolet, A.; Rosei, F. Photovoltaic Properties of Bi_2FeCrO_6 Epitaxial Thin Films. *Appl. Phys. Lett.* **2011**, *98*, 202902.
(25) Nechache, R.; Harnagea, C.; Li, S.; Cardenas, L.; Huang, W.; Chakrabartty, J.; Rosei, F. Bandgap Tuning of Multiferroic Oxide Solar Cells. *Nat. Photonics* **2014**, *9*, 61−67.
(26) Sipe, J. E.; Shkrebtii, A. I. Second-order Optical Response in Semiconductors. *Phys. Rev. B: Condens. Matter Mater. Phys.* **2000**, *61*, 5337−52.
(27) von Baltz, R.; Kraut, W. Theory of the bulk photovoltaic effect in pure crystals. *Phys. Rev. B: Condens. Matter Mater. Phys.* **1981**, *23*, 5590−6.
(28) Wang, F.; Young, S. M.; Zheng, F.; Grinberg, I.; Rappe, A. M. Substantial Bulk Photovoltaic Effect Enhancement Via Nanolayering. *Nat. Commun.* **2016**, *7*, 10419.
(29) Wang, F.; Rappe, A. M. First-principles Calculation of the Bulk Photovoltaic Effect in $KNbO_3$ and (K, Ba) (Ni, Nb)$O_{3-\delta}$. *Phys. Rev. B: Condens. Matter Mater. Phys.* **2015**, *91*, 165124.
(30) Young, S. M.; Zheng, F.; Rappe, A. M. First-principles Materials Design of High-performing Bulk Photovoltaics with the $LiNbO_3$ Structure. *Phys. Rev. Appl.* **2015**, *4*, 054004.
(31) Wang, F.; Grinberg, I.; Rappe, A. M. Semiconducting Ferroelectric Photovoltaics through Zn^{2+} Doping into $KNbO_3$ and Polarization Rotation. *Phys. Rev. B: Condens. Matter Mater. Phys.* **2014**, *89*, 235105.
(32) Wang, F.; Grinberg, I.; Rappe, A. M. Band Gap Engineering Strategy Via Polarization Rotation in Perovskite Ferroelectrics. *Appl. Phys. Lett.* **2014**, *104*, 152903.
(33) Jiang, L.; Grinberg, I.; Wang, F.; Young, S. M.; Davies, P. K.; Rappe, A. M. *Phys. Rev. B: Condens. Matter Mater. Phys.* **2014**, *90*, 075153.
(34) Catalan, G.; Scott, J. F. Physics and Applications of Bismuth Ferrite. *Adv. Mater.* **2009**, *21*, 2463−2485.
(35) Burroughes, J. H.; Bradley, D. D. C.; Brown, A. R.; Marks, R. N.; Mackay, K.; Friend, R. H.; Burns, P. L.; Holmes, A. B. Light-emitting Diodes Based on Conjugated Polymers. *Nature* **1990**, *347*, 539−541.
(36) Friend, R. H.; Gymer, R. W.; Holmes, A. B.; Burroughes, J. H.; Marks, R. N.; Taliani, C.; Bradley, D. D. C.; Santos, D. A. D.; Brdas, J. L.; Lgdlund, M.; Salaneck, W. R. Electroluminescence in Conjugated Polymers. *Nature* **1999**, *397*, 121−128.
(37) Chen, S.; Teng, C.; Zhang, M.; Li, Y.; Xie, D.; Shi, G. A Flexible UV-Vis-NIR Photodetector based on a Perovskite/Conjugated-Polymer Composite. *Adv. Mater.* **2016**, *28*, 5969−5974.
(38) Sirringhaus, H.; Kawase, T.; Friend, R. H.; Shimoda, T.; Inbasekaran, M.; Wu, W.; Woo, E. P. High-Resolution Inkjet Printing of All-Polymer Transistor Circuits. *Science* **2000**, *290*, 2123−2126.
(39) Tseng, H.-R.; Phan, H.; Luo, C.; Wang, M.; Perez, L. A.; Patel, S. N.; Ying, L.; Kramer, E. J.; Nguyen, T.-Q.; Bazan, G. C.; Heeger, A. J. High-Mobility Field-Effect Transistors Fabricated with Macroscopic Aligned Semiconducting Polymers. *Adv. Mater.* **2014**, *26*, 2993−2998.
(40) Lei, T.; Dou, J.-H.; Ma, Z.-J.; Yao, C.-H.; Liu, C.-J.; Wang, J.-Y.; Pei, J. Ambipolar Polymer Field-Effect Transistors Based on Fluorinated Isoindigo: High Performance and Improved Ambie nt Stability. *J. Am. Chem. Soc.* **2012**, *134*, 20025−20028.
(41) Dou, L.; Liu, Y.; Hong, Z.; Li, G.; Yang, Y. Low-Bandgap Near-IR Conjugated Polymers/Molecules for Organic Electronics. *Chem. Rev.* **2015**, *115*, 12633−12665.
(42) SambathKumar, B.; Kumar, P. S. V.; Deepakrao, F. S.; Iyer, S. S. K.; Subramanian, V.; Datt, R.; Gupta, V.; Chand, S.; Somanathan, N. Two Donor−One Acceptor Random Terpolymer Comprised of Diketopyrrolopyrrole Quaterthiophene with Various Donor *pi*-Linkers for Organic Photovoltaic Application. *J. Phys. Chem. C* **2016**, *120*, 26609−26619.
(43) Park, S. H.; Roy, A.; Beaupr, S.; Cho, S.; Coates, N.; Moon, J. S.; Moses, D.; Leclerc, M.; Lee, K.; Heeger, A. J. Bulk Heterojunction Solar Cells with Internal Quantum Efficiency Approaching 100%. *Nat. Photonics* **2009**, *3*, 297−302.
(44) van Mullekom, H. Developments in the Chemistry and Band Gap Engineering of Donor−acceptor Substituted Conjugated Polymers. *Mater. Sci. Eng., R* **2001**, *32*, 1−40.
(45) Zhou, Z.-H.; Maruyama, T.; Kanbara, T.; Ikeda, T.; Ichimura, K.; Yamamoto, T.; Tokuda, K. Unique Optical and Electrochemical Properties of π-conjugated Electrically Conducting Copolymers Consisting of Electron-withdrawing Pyridine Units and Electron-donating Thiophene Units. *J. Chem. Soc., Chem. Commun.* **1991**, 1210−1212.
(46) Cheng, Y.-J.; Yang, S.-H.; Hsu, C.-S. Synthesis of Conjugated Polymers for Organic Solar Cell Applications. *Chem. Rev.* **2009**, *109*, 5868−5923.
(47) Dahlstrand, C.; Jahn, B. O.; Grigoriev, A.; Villaume, S.; Ahuja, R.; Ottosson, H. Polyfulvenes: Polymers with "Handles" That Enable

DOI: 10.1021/acs.jpcc.7b00374
J. Phys. Chem. C 2017, 121, 6500−6507

Extensive Electronic Structure Tuning. *J. Phys. Chem. C* **2015**, *119*, 25726−25737.
(48) Wong, B. M.; Cordaro, J. G. Electronic Properties of Vinylene-Linked Heterocyclic Conducting Polymers: Predictive Design and Rational Guidan ce from DFT Calculations. *J. Phys. Chem. C* **2011**, *115*, 18333−18341.
(49) Ogden, T. R.; Gookin, D. M. Bulk Photovoltaic Effect in Polyvinylidene Fluoride. *Appl. Phys. Lett.* **1984**, *45*, 995.
(50) Brehm, J. A.; Young, S. M.; Zheng, F.; Rappe, A. M. First-principles Calculation of the Bulk Photovoltaic Effect in the Polar Compounds $LiAsS_2$, $LiAsSe_2$, and $NaAsSe_2$. *J. Chem. Phys.* **2014**, *141*, 204704.
(51) Zheng, F.; Takenaka, H.; Wang, F.; Koocher, N. Z.; Rappe, A. M. First-Principles Calculation of Bulk Photovoltaic Effect in $CH_3NH_3PbI_3$ and $CH_3NH_3PbI_{3-x}Cl_x$. *J. Phys. Chem. Lett.* **2015**, *6*, 31−37.
(52) Tan, L. Z.; Rappe, A. M. Enhancement of the Bulk Photovoltaic Effect in Topological Insulators. *Phys. Rev. Lett.* **2016**, *116*, 237402.
(53) Rangel, T.; Fregoso, B. M.; Mendoza, B. S.; Morimoto, T.; Moore, J. E.; Neaton, J. B. Giant Bulk Photovoltaic Effect and Spontaneous Polarization of Single-layer Monochalcogenides. arXiv preprint arXiv:1610.06589, 2016.
(54) Tan, L. Z.; Zheng, F.; Young, S. M.; Wang, F.; Liu, S.; Rappe, A. M. Shift Current Bulk Photovoltaic Effect in Polar Materials—hybrid and Oxide Perovskites and Beyond. *npj Comput. Mater.* **2016**, *2*, 16026.
(55) Perdew, J. P.; Burke, K.; Ernzerhof, M. Generalized Gradient Approximation Made Simple. *Phys. Rev. Lett.* **1996**, *77*, 3865−8.
(56) Rappe, A. M.; Rabe, K. M.; Kaxiras, E.; Joannopoulos, J. D. Optimized Pseudopotentials. *Phys. Rev. B: Condens. Matter Mater. Phys.* **1990**, *41*, 1227−30.
(57) Ramer, N. J.; Rappe, A. M. Designed Nonlocal Pseudopotentials for Enhanced Transferability. *Phys. Rev. B: Condens. Matter Mater. Phys.* **1999**, *59*, 12471−8.
(58) Heyd, J.; Scuseria, G. E.; Ernzerhof, M. Erratum: "Hybrid functionals based on a screened Coulomb potential". *J. Chem. Phys.* **2006**, *124*, 154709, and erratum: J. Chem. Phys. 125, 249901 (2006)
(59) Becke, A. Density-functional Thermochemistry. III. the Role of Exact Exchange. *J. Chem. Phys.* **1993**, *98*, 5648−52.
(60) Spataru, C. D.; Ismail-Beigi, S.; Benedict, L. X.; Louie, S. G. Excitonic Effects and Optical Spectra of Single-Walled Carbon Nanotubes. *Phys. Rev. Lett.* **2004**, *92*, 077402.
(61) Morimoto, T.; Nagaosa, N. Topological aspects of nonlinear excitonic processes in noncentrosymmetric crystals. *Phys. Rev. B: Condens. Matter Mater. Phys.* **2016**, *94*, 035117.

DOI: 10.1021/acs.jpcc.7b00374
J. Phys. Chem. C 2017, 121, 6500−6507